

Use of $V_{\text{low-k}}$ in a chiral-perturbation-theory description of the $pp \rightarrow pp\pi^0$ reaction

Y. Kim^{(a)1}, I. Danchev^{(a)2}, K. Kubodera^{(a)3}, F. Myhrer^{(a)4} T. Sato^{(b)5}

^(a) *Department of Physics and Astronomy,*

University of South Carolina, Columbia, SC 29208, USA

^(b) *Department of Physics, Osaka University, Toyonaka, Osaka 560, Japan*

Previously, the near-threshold $pp \rightarrow pp\pi^0$ reaction was studied with the use of transition operators derived from chiral perturbation theory (χ PT) and the nuclear wave functions generated by high-precision phenomenological potentials. A conceptual problem in that approach was that the transition amplitude receives contributions from very high momentum components (above the cutoff scale of χ PT) in the nuclear wave functions. In the present work, we avoid this problem by replacing the “bare” phenomenological potentials with $V_{\text{low-k}}$, which is an effective potential derived from a bare potential by integrating out momentum components higher than a specified cutoff scale. The use of $V_{\text{low-k}}$ is found to give an enhancement of the $pp \rightarrow pp\pi^0$ cross sections over the values obtained with bare potentials. Although this enhancement brings the calculated cross sections closer to the experimental values, the incident-energy dependence of the cross section is not well reproduced, a problem that seems to indicate the necessity of including higher chiral order terms than considered in the present work.

¹E-mail: ykim@physics.sc.edu

²E-mail: danchev@physics.sc.edu

³E-mail: kubodera@sc.edu

⁴E-mail: myhrer@sc.edu

⁵E-mail: tsato@phys.sci.osaka-u.ac.jp

1 Introduction

There have been many theoretical investigations [1]-[13] devoted to explaining the high-precision data for the total cross section of the near-threshold $pp \rightarrow pp\pi^0$ reaction [14, 15]. The initial surprise was that the measured cross section was larger than the values expected from the earlier calculations [16, 17] by a factor of ~ 5 . Calculations in the phenomenological one-boson-exchange model indicated that heavy-meson (σ and ω) exchange contributions could account for the unexpectedly large cross section for $pp \rightarrow pp\pi^0$ [1]. The importance of heavy-meson exchanges in π^0 production is to be contrasted with their much less pronounced role in the charged-pion production process, which is dominated by the one-pion-exchange diagrams. Effective field theory (EFT), or more specifically, chiral perturbation theory (χ PT) offers a systematic framework for describing the $NN \rightarrow NN\pi$ processes at low energies. The leading-order term in χ PT (the Weinberg-Tomozawa term) contributes to charged-pion production but not to π^0 production. χ PT allows us to keep track of the contributions of higher chiral-order terms to the low-energy $NN \rightarrow NN\pi$ reactions [4, 5]. A point to be kept in mind, however, is that the $NN \rightarrow NN\pi$ processes involve rather large momentum transfers, $p \sim \sqrt{m_N m_\pi}$ ($m_N =$ nucleon mass, $m_\pi =$ pion mass) even at threshold, and that this feature leads to the relatively slow convergence of the χ PT expansion [6]. The existence of the additional scale $p \sim \sqrt{m_N m_\pi}$ in the $NN \rightarrow NN\pi$ reaction led Cohen et al.[5, 11] to propose a new counting scheme in which the expansion parameter is $\chi \equiv \sqrt{m_\pi/m_N}$ instead of $\chi_W \equiv m_\pi/m_N$ employed in the usual Weinberg counting scheme. A thorough discussion on this and related topics as well as an extensive list of references can be found in a recent review by Hanhart [13].

To maintain formal consistency in the χ PT calculation of an inelastic nuclear process, one should derive from the same effective Lagrangian the relevant transition operators and the wave functions for the initial and final nuclear states. This type of calculation, however, has not yet been carried out. A practical and, in many cases, very useful method is a hybrid χ PT approach [18]-[22], in which the transition operators are derived from χ PT but the nuclear wave functions are generated with the use of a modern high-precision phenomenological N-N potential. Hybrid χ PT was applied to the $pp \rightarrow pp\pi^0$ reaction in Refs. [4]-[8]. These studies indicated: (1) There is a substantial cancellation between the one-body impulse approximation (IA) term and the two-body contributions, resulting in a cross section that is much smaller than the experimental value; (2) This feature seems reasonably stable against the different choices of phenomenological NN-potentials.¹

A conceptual problem one encounters in these hybrid χ PT calculations is that, whereas the transition operators are derived using χ PT with the assumption that relevant momenta are sufficiently small compared with the chiral scale Λ_χ ($p \ll \Lambda_\chi \approx 1$ GeV), the wave functions generated by a phenomenological N-N potential can in principle contain momenta of any magnitude. A numerical calculation in Ref. [7] indicates that the transition amplitude receives non-negligible contributions from momentum components well above Λ_χ , a feature that jeopardizes the applicability of χ PT.

In a version of hybrid χ PT called EFT* or MEEFT [19]-[21], the contribution of the dangerously high momentum components in the wave functions are suppressed by attaching a momentum cutoff factor to the transition operators derived from χ PT.² EFT* has proved to be extremely useful in

¹Ref. [7] reports that the two different N-N potentials, Argonne V18 [23] and Reid soft-core [24], give almost the same results for the $pp \rightarrow pp\pi^0$ cross sections.

²Another important aspect of EFT* is that the low-energy constants appearing in the theory are constrained by the experimental data for the observables involving neighboring nuclei. This aspect of EFT*, however, will not be discussed

explaining and predicting many important observables for electroweak processes in few-nucleon systems. Another possible way to suppress the contributions of high momentum components in hybrid χ PT calculations is to attach a momentum cutoff factor to the wave functions.³ Meanwhile, a systematic method was developed by the Stony Brook group and others [25, 26] to construct from a phenomenological NN-potential an *effective* NN potential that resides in a model space which only contains momentum components below a specified cutoff scale Λ . This effective potential, referred to as $V_{\text{low-}k}$, is obtained by integrating out momentum components higher than Λ from a phenomenological NN-potential, which in this context may be regarded as an underlying “bare” potential that resides in full momentum space. $V_{\text{low-}k}$ represents a renormalization-group-improved effective interaction of a bare NN interaction. It has been found that, for a choice of $\Lambda \sim 2 \text{ fm}^{-1}$, $V_{\text{low-}k}$ reproduces low-energy observables such as the phase shifts (for $p < \Lambda$) and the deuteron binding energy with accuracy comparable to that achieved with the use of bare high-precision phenomenological potentials [26]. Furthermore, for any choice of bare NN-interactions (belonging to the category of modern high-precision phenomenological potentials), it has been found that the corresponding $V_{\text{low-}k}$ generates practically the same half-off-shell T-matrix elements for $p < \Lambda$. This means that the low-momentum behavior ($p < \Lambda$) of the two-nucleon wave functions calculated from $V_{\text{low-}k}$ is essentially model-independent.

These developments motivate us to carry out a hybrid χ PT calculation of the near-threshold $pp \rightarrow pp\pi^0$ reaction with the use of $V_{\text{low-}k}$. This type of calculation will substantially reduce the severity of the conceptual problem of momentum component mismatching that existed in the previous hybrid χ PT calculations. It will thus allow us to examine more directly whether the transition operators derived from χ PT up to a given chiral order are adequate or not. Furthermore, comparison of the results of a calculation based on $V_{\text{low-}k}$ with those based on bare NN-interactions will also give information about the influences of the short-distance behavior of the NN-interactions on the $NN \rightarrow NN\pi$ reactions. In this context, it is informative to gather more examples of calculations that use bare NN-interactions. Therefore, in addition to a calculation based on $V_{\text{low-}k}$, we extend here our previous bare-potential-based calculations (carried out for the Argonne V18 and Reid soft-core potentials) to the Bonn-B potential [34] and the CD Bonn potential [33].

After describing the primary motivations of our work, we must mention that our present study is basically of exploratory nature and falls short of addressing a number of issues that warrant detailed studies. For one thing, we limit ourselves to the use of the Weinberg counting scheme, although it is important to examine the consequences of the counting scheme of Refs. [5, 11]. As for the employment of $V_{\text{low-}k}$ in hybrid χ PT, there is a problem of formal consistency in that, whereas the relevant transition operators are derived in the framework of the dimensional regularization [4, 7], $V_{\text{low-}k}$ is based on the momentum cutoff scheme. Furthermore, the difference between the cutoff scales appearing in Ref. [7] and in $V_{\text{low-}k}$ needs to be addressed. We relegate the study of these points to future work and concentrate on the examination of the consequences of the use of $V_{\text{low-}k}$ in the present limited context; on the last point, however, we will give some brief remarks later in the text.

The organization of this paper is as follows. Sect. 2 gives a brief recapitulation of the general framework of hybrid χ PT, while we explain in Sect.3 some technical aspects of numerical calculations we need to address as we work with $V_{\text{low-}k}$ instead of the bare potential. The numerical results are presented in

here.

³Insofar as the use of a momentum cutoff factor can be identified with the introduction of a projection operator onto a model space with a limited momentum range, applying the cutoff factor to the transition operators is equivalent to applying it to the wave functions.

Sect. 4 and compared with the data. Finally, Sect. 5 is dedicated to discussion and summary.

2 Calculational Framework

The formalism to be used here is basically the same as in Refs. [4, 7] except that, for a calculation with $V_{\text{low-k}}$, some modifications (essentially of technical nature) are needed. Therefore, as far as the general framework of our approach is concerned, we only give a brief recapitulation, referring to Refs. [4, 7] for details.

2.1 Transition operators

As in Refs. [4, 7], we derive the transition operators for the $pp \rightarrow pp\pi^0$ reaction using the heavy-fermion formalism (HFF) [27] of χ PT based on the Weinberg counting rules. The relevant lagrangian is written as

$$\mathcal{L}_{\text{ch}} = \mathcal{L}^{(0)} + \mathcal{L}^{(1)} + \mathcal{L}^{(2)} + \dots \quad (1)$$

Here $\mathcal{L}^{(\bar{\nu})}$ ($\bar{\nu} = 0, 1, 2, \dots$) contains terms of chiral order $\bar{\nu}$ with $\bar{\nu} \equiv d + (n/2) - 2$, where n is the number of fermion lines involved in the vertex and d is the number of derivatives or powers of m_π . For our present study we only need the terms of $\bar{\nu} = 0$ and $\bar{\nu} = 1$, which are given as follows:

$$\mathcal{L}^{(0)} = \frac{f_\pi^2}{4} \text{Tr}[\partial_\mu U^\dagger \partial^\mu U + m_\pi^2 (U^\dagger + U - 2)] + \bar{N}(iv \cdot D + g_A S \cdot u)N \quad (2)$$

$$\begin{aligned} \mathcal{L}^{(1)} = & -\frac{ig_A}{2m_N} \bar{N}\{S \cdot D, v \cdot u\}N + 2c_1 m_\pi^2 \bar{N}N \text{Tr}(U + U^\dagger - 2) \\ & + (c_2 - \frac{g_A^2}{8m_N}) \bar{N}(v \cdot u)^2 N + c_3 \bar{N}u \cdot uN. \end{aligned} \quad (3)$$

Here $U(x)$ is an SU(2) matrix that is non-linearly related to the pion field and that has standard chiral transformation properties; we use $U(x) = \sqrt{1 - [\vec{\pi}(x)/f_\pi]^2} + i\vec{\tau} \cdot \vec{\pi}(x)/f_\pi$. $N(x)$ denotes the large component of the heavy-fermion field; the four-velocity parameter v_μ is chosen to be $v_\mu = (1, 0, 0, 0)$. $D_\mu N$ is the covariant derivative, S_μ is the covariant spin operator, and $u_\mu \equiv i[\xi^\dagger \partial_\mu \xi - \xi \partial_\mu \xi^\dagger]$, where $\xi = \sqrt{U(x)}$ [28]. The pion decay constant is taken to be $f_\pi = 93$ MeV, and $g_A = 1.25$. The values of the low-energy constants (LECs), c_1, c_2 and c_3 , are given in, e.g., Refs. [4, 28, 29]:

$$c_1 = -0.87 \pm 0.11 \text{ GeV}^{-1}, \quad c_2 = 3.34 \pm 0.27 \text{ GeV}^{-1}, \quad c_3 = -5.25 \pm 0.22 \text{ GeV}^{-1}. \quad (4)$$

The chiral order index ν of a Feynman diagram is defined by $\nu = 4 - E_N - 2C + 2L + \sum_i \bar{\nu}_i$, where E_N is the number of nucleons in the Feynman diagram, L the number of loops, C the number of disconnected parts in the diagram, and the sum runs over all the vertices in the Feynman graph [30]. We are using here the Weinberg counting scheme [30], although, as mentioned in the introduction, there exists a different counting scheme tailored to keep track of high-momentum flows involved in $NN \rightarrow NN\pi$ reactions [5, 13]. Furthermore, we limit ourselves to the tree-level diagrams and examine the consequences of employing $V_{\text{low-k}}$ in evaluating the transition matrix elements corresponding to these tree diagrams.

The kinematic variables for the $pp \rightarrow pp\pi^0$ reaction we use in this work and the relevant Feynman diagrams are shown in Fig. 1. As discussed in Refs. [4, 7], the lagrangian in Eq. (1) leads to the transition operator

$$\mathcal{T} = \mathcal{T}^{(-1)} + \mathcal{T}^{(+1)} \equiv \mathcal{T}^{(\text{Imp})} + \mathcal{T}^{(\text{Resc})}, \quad (5)$$

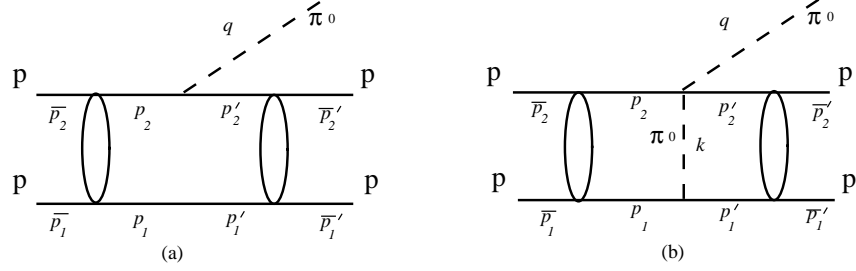


Figure 1: Impulse term (a) and rescattering term (b) for the $pp \rightarrow pp\pi^0$ reaction. In the text, the space components of the initial four-momenta \vec{p}_1 and \vec{p}_2 in the center-of-mass system are denoted by \vec{p}_i and $-\vec{p}_i$, respectively; similarly, the space components of the final four-momenta \vec{p}'_1 and \vec{p}'_2 in the center-of-mass system are denoted by $\vec{p}_f - \vec{q}/2$ and $-\vec{p}_f - \vec{q}/2$, respectively.

where $\mathcal{T}^{(\nu)}$ represents the contribution of chiral order ν . $\mathcal{T}^{(-1)}$ comes from the one-body impulse approximation (IA) diagram [Fig. 1(a)] and is given by

$$\mathcal{T}^{(-1)} \equiv \mathcal{T}^{(\text{Imp})} \equiv \frac{i}{(2\pi)^{3/2}} \frac{1}{\sqrt{2\omega_q}} \frac{g_A}{2f_\pi} \sum_{j=1,2} [-\vec{\sigma}_j \cdot \vec{q} + \frac{\omega_q}{2m_N} \vec{\sigma}_j \cdot (\vec{p}_j + \vec{p}'_j)] \tau_j^0. \quad (6)$$

$\mathcal{T}^{(+1)}$, which arises from the two-body rescattering diagram [Fig.1(b)], is given by

$$\mathcal{T}^{(+1)} \equiv \mathcal{T}^{(\text{Resc})} \equiv \frac{-i}{(2\pi)^{9/2}} \frac{1}{\sqrt{2\omega_q}} \frac{g_A}{f_\pi} \sum_{j=1,2} \kappa(k_j, q) \frac{\vec{\sigma}_j \cdot \vec{k}_j}{k_j^2 - m_\pi^2} \tau_j^0, \quad (7)$$

where \vec{p}_j and \vec{p}'_j ($j = 1, 2$) denote the initial and final momenta of the j -th proton. The four-momentum of the exchanged pion is defined by the nucleon four-momenta at the πNN vertex as $k_j \equiv p_j - p'_j$, where $p_j = (E_{p_j}, \vec{p}_j)$, $p'_j = (E_{p'_j}, \vec{p}'_j)$ with $E_p \equiv (\vec{p}^2 + m_N^2)^{1/2}$. The four-momenta of the final pion is $q = (\omega_q, \vec{q})$, with $\omega_q = (\vec{q}^2 + m_\pi^2)^{1/2}$. The rescattering vertex function $\kappa(k, q)$ of Eq.(7) is calculated from Eq.(3):

$$\kappa(k, q) \equiv \frac{m_\pi^2}{f_\pi^2} [2c_1 - (c_2 - \frac{g_A^2}{8m_N}) \frac{\omega_q k_0}{m_\pi^2} - c_3 \frac{q \cdot k}{m_\pi^2}], \quad (8)$$

where $k = (k_0, \vec{k})$ represents the four-momenta of the exchanged pion.

2.2 Transition amplitude and nuclear wave functions

We write the transition amplitude for the $pp \rightarrow pp\pi^0$ reaction as

$$T = \langle \Phi_f | \mathcal{T} | \Phi_i \rangle, \quad (9)$$

where $|\Phi_i\rangle$ ($|\Phi_f\rangle$) is the initial (final) two-nucleon state distorted by the initial-state (final-state) interaction. As briefly discussed in the introduction, in a formally consistent nuclear χ PT calculation, the transition operator \mathcal{T} and the N-N interactions that generate $|\Phi_i\rangle$ and $|\Phi_f\rangle$ are to be calculated to the same chiral order ν from the common χ PT lagrangian. In hybrid χ PT, we instead use a phenomenological N-N potential to generate $|\Phi_i\rangle$ and $|\Phi_f\rangle$. In the present treatment this phenomenological N-N potential can be either $V_{\text{low-k}}$ or a bare NN-interaction (see the introduction).

As described in Ref. [7], we can apply the standard partial-wave decomposition to Eq. (9) and rewrite it into

$$\begin{aligned} \langle \chi_{\vec{p}_f, m_{s'_1}, m_{s'_2}}^{(-)} \vec{q} | \mathcal{T} | \chi_{\vec{p}_i, m_{s_1}, m_{s_2}}^{(+)} \rangle &= \sum_{S_f L_f J_f M_f} \sum_{S_i L_i J_i M_i} \mathcal{Y}_{S_f L_f}^{J_f M_f^+}(\hat{p}_f, m_{s'_1}, m_{s'_2}) \mathcal{Y}_{S_i L_i}^{J_i M_i}(\hat{p}_i, m_{s_1}, m_{s_2}) \\ &\times \sum_{l_\pi m_\pi} Y_{l_\pi m_\pi}^*(\hat{q}) \langle p_f [L_f S_f] J_f M_f | \mathcal{T}_{l_\pi m_\pi}(q) | p_i [L_i S_i] J_i M_i \rangle, \end{aligned} \quad (10)$$

Here \mathcal{Y}_{SL}^{JM} is the spin-angular function of the antisymmetrized two-proton state

$$\mathcal{Y}_{SL}^{JM} \equiv \frac{1 + (-1)^{L+S}}{\sqrt{2}} \sum_{M_S M_L} i^L \exp[i\delta_{(LS)J}] Y_{LM_L}^*(\hat{p}) \langle \frac{1}{2} \frac{1}{2} m_{s_1} m_{s_2} | S M_S \rangle \langle L S M_L M_S | J M \rangle, \quad (11)$$

where $\delta_{(LS)J}$ is the NN scattering phase shift in the eigen-channel defined by the orbital angular momentum L , total spin S , and the total angular momentum J . l_π denotes the angular momentum of the outgoing pion. It is convenient to introduce the reduced matrix element using the standard convention:

$$\langle p_f [L_f S_f] J_f M_f | \mathcal{T}_{l_\pi m_\pi}(q) | p_i [L_i S_i] J_i M_i \rangle \quad (12)$$

$$\equiv (-1)^{J_f - M_f} \begin{pmatrix} J_f & l_\pi & J_i \\ -M_f & m_\pi & M_i \end{pmatrix} \langle p_f [L_f S_f] J_f || \mathcal{T}_{l_\pi m_\pi}(q) || p_i [L_i S_i] J_i \rangle. \quad (13)$$

Corresponding to the decomposition $\mathcal{T} = \mathcal{T}^{\text{Imp}} + \mathcal{T}^{\text{Resc}}$ in Eq.(5), the reduced matrix element has two terms

$$\begin{aligned} &\langle p_f [L_f S_f] J_f || \mathcal{T}_{l_\pi}(q) || p_i [L_i S_i] J_i \rangle \\ &= \langle p_f [L_f S_f] J_f || \mathcal{T}_{l_\pi}^{\text{Imp}}(q) || p_i [L_i S_i] J_i \rangle + \langle p_f [L_f S_f] J_f || \mathcal{T}_{l_\pi}^{\text{Resc}}(q) || p_i [L_i S_i] J_i \rangle. \end{aligned} \quad (14)$$

Near threshold we can assume that the $pp \rightarrow pp\pi^0$ reaction is dominated by s-wave pion production, with the final pp states in the 1S_0 partial wave; this implies that we need only consider the 3P_0 partial wave for the initial pp state. With these constraints, the reduced matrix elements for the impulse and rescattering terms are given by

$$\begin{aligned} \frac{1}{\sqrt{4\pi}} \langle p_f [^1S_0] || \mathcal{T}_{l_\pi=0}^{\text{Imp}}(q) || p_i [^3P_0] \rangle &= \frac{-i}{\sqrt{(2\pi)^3 2\omega_q}} \frac{g_A}{f_\pi} \int \int \frac{d\vec{p}' d\vec{p}}{4\pi} R_{^1S_0, p_f}(p') \\ &\times \hat{p} \cdot \left(-\vec{q} + \frac{\omega_q}{m_N} \vec{p}' \right) \delta(\vec{p}' - \vec{p} + \vec{q}/2) R_{^3P_0, p_i}(p), \end{aligned} \quad (15)$$

$$\begin{aligned} \frac{1}{\sqrt{4\pi}} \langle p_f [^1S_0] || \mathcal{T}_{l_\pi=0}^{\text{Resc}}(q) || p_i [^3P_0] \rangle &= \frac{i}{\sqrt{(2\pi)^3 2\omega_q}} \frac{2g_A}{f_\pi} \int \int \frac{d\vec{p}' d\vec{p}}{4\pi} R_{^1S_0, p_f}(p') \\ &\times \frac{\kappa(k, q)}{(2\pi)^3} \frac{\hat{p} \cdot \vec{k}}{k^2 - m_\pi^2} R_{^3P_0, p_i}(p). \end{aligned} \quad (16)$$

The radial functions, $R_{^3P_0, p_i}(p)$ and $R_{^1S_0, p_f}(p')$, in Eqs.(15) and (16) stand for the NN relative motion in the initial and final state, respectively. To obtain these radial functions, we first derive the K -matrix by solving the Lippman-Schwinger equation in momentum space for a given NN potential; see Ref. [31].

The calculated half-off-shell K -matrix and N-N phase shift $\delta_{(LS)J}$ give the corresponding momentum space radial wave function as:

$$R_{(LS)J,p_0}(p) = i^{-L} \cos(\delta_{(LS)J}) \left[\frac{\delta(p-p_0)}{p_0^2} + \mathcal{P} \frac{K_{(LS)J}(p, p_0, W)}{p_0^2/m_N - p^2/m_N} \right]. \quad (17)$$

Here \mathcal{P} means taking the principal-value part of the two-nucleon propagator, and p_0 is the on-shell momentum defined by $W = 2E_{p_0}$. We note that the on-shell K -matrix is related to the phase shift as $\tan(\delta_{(LS)J}) = -\pi p_0 m_N K_{(LS)J}(p_0, p_0)/2$.

The choice of the four-momentum k of the exchanged pion has been a subject of investigations in the literature, see e.g., Refs [4, 32]. In a simple prescription, which came to be known as fixed kinematics approximation (FKA) [4], we identify the four-momentums of the intermediate nucleon lines with the corresponding asymptotic values (ignoring thereby energy-momentum transfers due to the initial and final state interactions) and ‘‘freeze’’ all the kinematic variables at their threshold values. Thus FKA consists in using, in Eqs.(8) and (16), $k = (k_0, \vec{k}) = (m_\pi/2, \vec{k})$, $\vec{k} = \vec{p} - \vec{p}'$, and $q = (\omega_q, \vec{q}) = (m_\pi, \vec{0})$. Meanwhile, in Ref. [7], k was chosen in such a manner that energy-momentum conservation at each vertex in Fig.1(b) should be satisfied, *i.e.*,

$$k = (k_0, \vec{k}) = (E_{\vec{p}} - E_{\vec{p}' - \vec{q}/2}, \vec{p} - \vec{p}' + \vec{q}/2), \quad (18)$$

where \vec{p} (\vec{p}') is the relative momentum of the two protons before (after) pion emission, defined in Fig. 1 as:

$$\vec{p}_1 = -\vec{p}_2 = \vec{p}, \quad \vec{p}'_1 = \vec{p}' - \frac{\vec{q}}{2}, \quad \vec{p}'_2 = -\vec{p}' - \frac{\vec{q}}{2}. \quad (19)$$

A schematic study in Ref. [32] indicates that, when the final-state NN interaction is included in the rescattering diagram, FKA is an appropriate choice, but that, when initial-state interaction is included, the situation is more complex. Thus the choice of k is still an open issue. In the present work therefore we give numerical results for the choice of k given in Eqs.(18) and (19), as well as for FKA. The bulk of our calculation will be done with the use of k given in Eqs.(18) and (19); the results corresponding to FKA will be presented with due remarks attached to them.

2.3 Cross sections

The total cross section at energy $W (= 2E_{\vec{p}_i})$ in the center-of-mass frame for the reaction $pp \rightarrow pp\pi^0$ is given by [7]

$$\begin{aligned} \sigma_{pp \rightarrow pp\pi^0}(W) &= \frac{(2\pi)^4 E_{p_i}}{16 p_i} \int_0^{q_m} dq q^2 p_f \sqrt{4E_{p_f}^2 + \vec{q}^2} \\ &\times \sum_{L_i S_i J_i L_f S_f J_f l_\pi} \left| \frac{1}{\sqrt{4\pi}} e^{i\delta(L_f S_f)J_f + i\delta(L_i S_i)J_i} \langle p_f [L_f S_f] J_f || \mathcal{T}_{l_\pi}(q) || p_i [L_i S_i] J_i \rangle \right|^2 \end{aligned} \quad (20)$$

where $E_{p_f} \equiv \{(W - \omega_q)^2 - \vec{q}^2\}^{1/2}/2$, $p_f \equiv \sqrt{E_{p_f}^2 - m_N^2}$, and the maximum momentum, q_m , of the pion is given by $q_m = \sqrt{\{(W - 2m_N)^2 - m_\pi^2\}\{(W + 2m_N)^2 - m_\pi^2\}/4W^2}$. Here p_i ($= |\vec{p}_i|$) is the asymptotic relative momentum of the initial pp states and $E_{\vec{p}_i} = \sqrt{\vec{p}_i^2 + m_N^2}$. Since we have already specialized ourselves in the threshold pion production, we need not deal with the general expression in Eq.(20); we can limit $[L_f S_f] J_f$ to 1S_0 and $[L_i S_i] J_i$ to 3P_0 .

2.4 NN interactions

As discussed in the introduction, the main purpose of the present work is to carry out a hybrid χ PT calculation of the $pp \rightarrow pp\pi^0$ reaction with the use of $V_{\text{low-}k}$, which resides in reduced Hilbert space characterized by the constraint $p < \Lambda$. Specifically, we use here the $V_{\text{low-}k}$ derived from the CD-Bonn potential [33].⁴ We are also interested in comparing the the results of this calculation with those of hybrid χ PT calculations based on standard high-precision phenomenological potentials, which we refer to as “bare” interactions. Regarding a bare NN potential case, in order to augment the examples given in Ref. [7], we shall carry out additional calculations with the use of the Bonn-B potential and the CD Bonn potential.

3 Numerical Calculation

The numerical evaluation of the scattering amplitude and the cross section follows closely the method employed in Ref. [7]. The calculation of the rescattering amplitude [Eq. (16)] can be readily done in momentum (p)-space, whereas it is technically easier to carry out a numerical evaluation of the impulse amplitude [Eq.(15)] in coordinate (r)-space [7]. Since the calculational method for the case of a bare NN-potential was explained in detail in Ref. [7], we only describe here modifications that need to be made when we use $V_{\text{low-}k}$ instead of a bare potential.

3.1 Principal-value integral

The principal value integral appearing in Eq. (17) is usually rendered amenable to numerical calculation in the following manner. If we need to numerically evaluate the integral

$$I \equiv \mathcal{P} \int_0^\infty dk \frac{f(k)}{q^2 - k^2}, \quad (21)$$

we may convert this expression into an ordinary integral by subtracting zero:

$$\begin{aligned} I &= \mathcal{P} \int_0^\infty dk \frac{f(k)}{q^2 - k^2} - \mathcal{P} \int_0^\infty dk \frac{f(q)}{q^2 - k^2} \\ &= \int_0^\infty dk \frac{1}{q^2 - k^2} [f(k) - f(q)]. \end{aligned} \quad (22)$$

In a calculation that involves $V_{\text{low-}k}$, the upper limit of k -integration is a finite value (Λ), so that we encounter an integral like

$$I_\Lambda \equiv \mathcal{P} \int_0^\Lambda dk \frac{f(k)}{q^2 - k^2}, \quad (23)$$

where, for the sake of definiteness, we may assume $q < \Lambda$. Since $\mathcal{P} \int_0^\Lambda dk \frac{f(q)}{q^2 - k^2} \neq 0$, the procedure used for I needs to be modified as

$$\begin{aligned} I_\Lambda &= \mathcal{P} \int_0^\Lambda dk \frac{f(k)}{q^2 - k^2} - \mathcal{P} \int_0^\Lambda dk \frac{f(q)}{q^2 - k^2} + \mathcal{P} \int_0^\Lambda dk \frac{f(q)}{q^2 - k^2} \\ &= \int_0^\Lambda dk \frac{1}{q^2 - k^2} [f(k) - f(q)] + \frac{f(q)}{2q} \log \frac{\Lambda + q}{\Lambda - q}. \end{aligned} \quad (24)$$

⁴We are grateful to T.T.S. Kuo for allowing us to use a computer code to generate $V_{\text{low-}k}$ developed by his group.

3.2 Calculation of the impulse-term amplitude in r-space.

As mentioned, the numerical evaluation of the impulse-term amplitude can be done more conveniently in r-space than in p-space. In a case involving a bare potential, switching from the p-representation to the r-representation can be readily performed using the standard Bessel transformation,

$$R_{(LS)J,p_0}(r) = \sqrt{\frac{2}{\pi}} i^L \int_0^\infty p^2 dp j_L(pr) R_{(LS)J,p_0}(p), \quad (25)$$

and the well-known identity, $\int_0^\infty j_L(pr) j_L(pr') p^2 dp = \frac{\pi}{2r^2} \delta(r - r')$. The result is given by [7]

$$\begin{aligned} \frac{1}{\sqrt{4\pi}} \langle p_f [^1S_0] || \mathcal{T}_{l_\pi=0}^{\text{Imp}}(q) || p_i [^3P_0] \rangle &= \frac{1}{\sqrt{(2\pi)^3 2\omega_q}} \frac{g_A}{f_\pi} \int dr r^2 R_{1S_0,p_f}(r) \\ &\times \left[\left(1 + \frac{\omega_q}{2m_N}\right) q j_1(qr/2) - \frac{\omega_q}{m_N} j_0(qr/2) \left(\frac{d}{dr} + \frac{2}{r}\right) \right] R_{3P_0,p_i}(r). \end{aligned} \quad (26)$$

The usefulness of this method, however, diminishes in the case of $V_{\text{low-k}}$, where the momentum integral does not run to ∞ but stops at Λ , and hence we cannot use the above-quoted orthogonality of the spherical Bessel functions: $\int_0^\Lambda j_L(pr) j_L(pr') p^2 dp \neq \frac{\pi}{2r^2} \delta(r - r')$. We therefore use the following procedure. In evaluating the impulse amplitude [Eq.(15)] for $V_{\text{low-k}}$, we first integrate out the δ -function, and then divide the range of p -integration in two intervals as follows.

$$\begin{aligned} \frac{1}{\sqrt{4\pi}} \langle p_f [^1S_0] || \mathcal{T}_{l_\pi=0}^{\text{Imp}}(q) || p_i [^3P_0] \rangle &= \frac{-i}{\sqrt{(2\pi)^3 2\omega_q}} \frac{g_A}{2f_\pi} \\ &\times \left\{ \int_0^{p_c} dp p^2 \int_{-1}^{+1} dx R_{1S_0,p_f}(p) \left[\frac{\vec{l}}{l} \cdot \left(-\vec{q} + \frac{\omega_q}{m_N} \vec{p}\right) \right] R_{3P_0,p_i}(l) \right. \\ &\quad \left. + \int_{p_c}^\Lambda dp p^2 \int_{-1}^{+1} dx R_{1S_0,p_f}(p) \left[\frac{\vec{l}}{l} \cdot \left(-\vec{q} + \frac{\omega_q}{m_N} \vec{p}\right) \right] R_{3P_0,p_i}(l) \right\}. \end{aligned} \quad (27)$$

Here $p = |\vec{p}|$, and x denotes the cosine of the angle between \vec{p} and \vec{q} , i.e., $\vec{p} \cdot \vec{q} = pqx$; $\vec{l} \equiv \vec{p} + \vec{q}/2$, and the momentum p_c is chosen to lie between p_f and p_m , where p_m is the solution of the equation $p = \sqrt{p_m^2 + p_m qx + q^2/4}$ for a given value of x . The merit of dividing the p-integration range in the two intervals is that each p -space integral in Eq.(27) contains only one principal-value part coming from either the initial or the final NN relative-motion propagator. For instance, in the second integral of Eq.(27) the final state radial wave function takes the following simple form

$$R_{1S_0,p_f}(p) = \cos[\delta(^1S_0)] m_N \frac{K_{1S_0}(p,p_f)}{p_f^2 - p^2},$$

where $p_f (< p_c)$ is the final-state on-shell momentum. We evaluate the first term in Eq.(27) directly in p -space. The second integral in Eq.(27) is calculated using a modified Bessel transformation outlined in the appendix.

Since the above-described method for carrying out the r-space calculation of the 1-body amplitude with $V_{\text{low-k}}$ is somewhat involved, it seems safer to check its validity using some pilot calculation. If in deriving \mathcal{T} we assume $\vec{q} = 0$ (the “ $\vec{q} = 0$ approximation”), the evaluation of the transition matrix element is drastically simplified, and even with $V_{\text{low-k}}$ we need not resort to the above lengthy prescription. We therefore consider it informative to compare the results of calculations with and without the “ $\vec{q} = 0$ approximation”. This comparison is given in Appendix B.

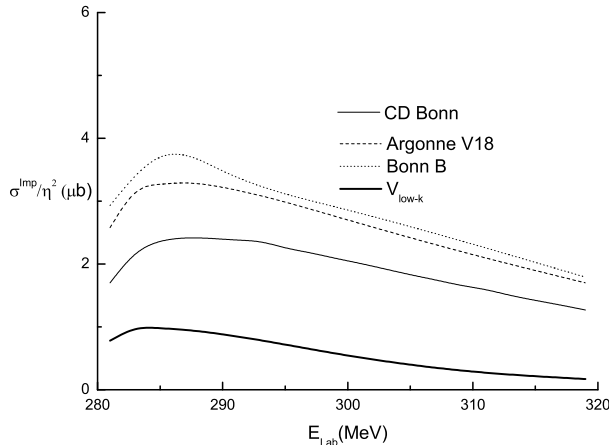


Figure 2: σ^{Imp} , the $pp \rightarrow pp\pi^0$ cross section calculated with the impulse term alone. The cross section is given in units of η^2 , where the “velocity” η is defined as the maximum pion momentum at a given laboratory energy E_{Lab} of the incident proton divided by the pion mass, $m_\pi = 135$ MeV.

4 Numerical Results

We now present the $pp \rightarrow pp\pi^0$ cross sections calculated with the use of $V_{\text{low-k}}$ [25] as well as typical bare NN interactions. We consider here three examples of the bare potential: Argonne V18 [23], Bonn-B [34], and CD-Bonn [33]. The results for Argonne V18 are taken from Ref. [7], while those for Bonn-B and CD-Bonn have been newly calculated in the present work. It is informative to study the individual behavior of the impulse- and rescattering-term contributions before discussing the behavior of their combined contributions.

4.1 Contribution of the impulse-approximation term

We first consider σ^{Imp} , the total $pp \rightarrow pp\pi^0$ cross section calculated with only the impulse-approximation amplitude retained; *viz.*, in evaluating Eq.(20), we replace $\langle p_f [L_f S_f] J_f || \mathcal{T}_\pi(q) || p_i [L_i S_i] J_i \rangle$ with $\langle p_f [^1S_0] || \mathcal{T}_{l_\pi=0}^{\text{Imp}}(q) || p_i [^3P_0] \rangle$. Fig. 2 shows σ^{Imp} as a function of E_{Lab} , the incident proton energy in the laboratory system. We note that, for the three representative bare NN-potentials, σ^{Imp} varies up to 40 %. These variations are a measure of ambiguity inherent in a calculation that uses a bare NN potential. The fact that the short-distance behavior of bare NN potentials is not controlled with sufficient accuracy underlies this instability. Fig. 2 indicates that the use of $V_{\text{low-k}}$ leads to a value of σ^{Imp} that is significantly smaller (by a factor of 3 or more) than those for the bare potentials. A plausible explanation of this difference is as follows. In the one-body transition diagram [Fig. 1(a)], the large momentum transfer ($p \sim \sqrt{m_\pi m_N}$) between the two nucleons needs to be mediated by the N-N potential.⁵ Now, by construction, $V_{\text{low-k}}$ only contains momentum components below $\Lambda = 2 \text{ fm}^{-1}$, whereas the bare potentials carry very high momentum components (albeit in a rather arbitrary manner). We can expect that the absence of those high-momentum components in $V_{\text{low-k}}$ suppresses the contribution of the one-body transition diagram.

⁵As pointed out in Ref.[7], with the use of a bare NN potential, one needs to take the upper limit of p -integration very high (up to $p \sim 2 \text{ GeV}/c$) before the integral starts to show a sign of convergence for both the impulse and rescattering amplitudes.

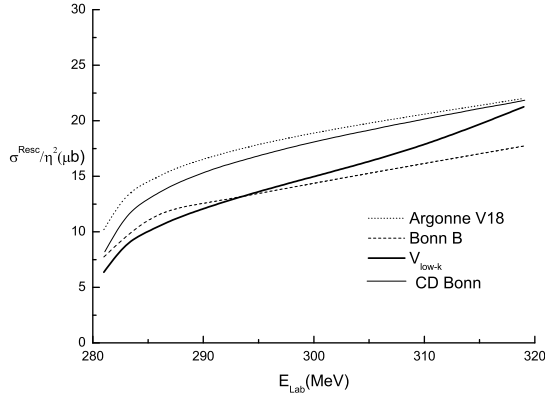


Figure 3: σ^{Resc} , the $pp \rightarrow pp\pi^0$ cross sections calculated with the rescattering term alone. For the explanation of the quantity η , see the caption of Fig.1.

As mentioned, we are using in the present work the $V_{\text{low-k}}$ derived from the CD Bonn potential. It is known, however, that, so long as one starts from a bare potential that belongs to the category of modern high-precision phenomenological potentials, the resulting $V_{\text{low-k}}$ is practically model-independent in the sense that the half-on-shell K -matrices corresponding to different bare potentials are nearly indistinguishable [25, 26]. This means that σ^{Imp} calculated with $V_{\text{low-k}}$ corresponding to any realistic bare potential would lie close to the solid line in Fig. 2. Thus the use of $V_{\text{low-k}}$ results in a significant reduction of model dependence in our calculation.

4.2 Contribution of the rescattering term

Fig. 3 gives σ^{Resc} , the total $pp \rightarrow pp\pi^0$ cross section calculated with only the rescattering term contribution retained; *i.e.*, in evaluating Eq.(20), we replace $\langle p_f[L_f S_f]J_f || \mathcal{T}_\pi(q) || p_i[L_i S_i]J_i \rangle$ with $\langle p_f[{}^1S_0] || \mathcal{T}_{l_\pi=0}^{\text{Resc}}(q) || p_i[{}^3P_0] \rangle$. The figure indicates that, for the three different choices of the bare NN-potential, σ^{Resc} shows variations of about 30 %, while the use of $V_{\text{low-k}}$ leads to σ^{Resc} that lies more or less within the range of these variations. In the rescattering diagram [Fig. 1(b)], a substantial fraction of the momentum transfer between the two nucleons can be carried by the exchanged pion, and therefore the NN interactions need not directly support a large momentum transfer. This feature explains why the change in σ^{Resc} is less pronounced than σ^{Imp} as we switch from the bare potentials to $V_{\text{low-k}}$. It is worth re-emphasizing here that, although $\sigma^{\text{Resc}}(V_{\text{low-k}})$ in Fig. 3 was obtained with the $V_{\text{low-k}}$ derived from the CD-Bonn potential, the result should be considered model-independent in the sense discussed in the preceding subsection.

4.3 Combined contributions of the impulse-approximation and rescattering terms

We now consider the total $pp \rightarrow pp\pi^0$ cross section, σ , calculated with the full transition amplitude consisting of the one-body and two-body terms; thus σ is obtained from Eq.(20) with the transition amplitude given by Eqs. (14), (15), (16). The results are shown in Fig. 4 for the three choices of the bare potential and for $V_{\text{low-k}}$, along with the experimental values of $\sigma_{pp \rightarrow pp\pi^0}$. Fig. 4 indicates that the use of $V_{\text{low-k}}$ leads to a rather visible enhancement of σ over the results obtained with the

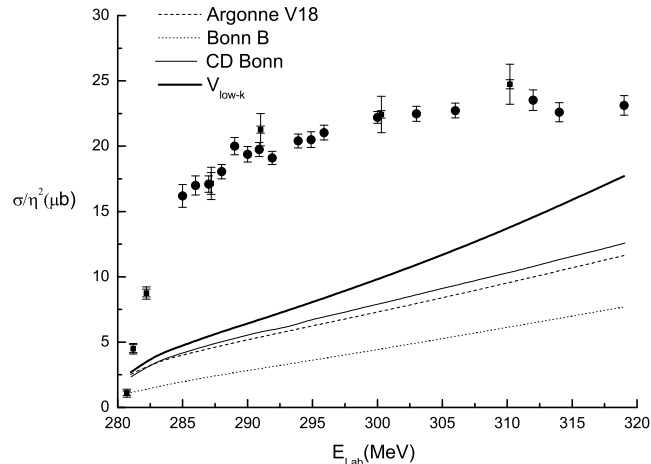


Figure 4: The total cross sections calculated from the full amplitude consisting of the impulse and rescattering terms. The experimental data points are taken from Ref. [14] (solid circles) and Ref. [15] (solid squares). For the explanation of the quantity η , see the caption of Fig.1.

bare potentials. This enhancement is related to the suppression of the impulse-approximation amplitude corresponding to $V_{\text{low-k}}$. As pointed out in the earlier χ PT calculations [4, 5], the impulse and rescattering amplitudes tend to interfere destructively, and in the case of a bare NN interaction the cancellation between the two amplitudes is quite substantial, leading to a significantly suppressed value of σ as compared with the individual magnitudes of σ^{Imp} and σ^{Resc} . The smaller impulse-approximation amplitude obtained with the use of $V_{\text{low-k}}$ somewhat diminishes the extent of this destructive interference, resulting in a larger value of σ . The enhancement of the cross section obtained with $V_{\text{low-k}}$ brings the calculated values of σ closer to the experimental values. It is to be noted, however, that the energy dependence of σ obtained with $V_{\text{low-k}}$ differs significantly from the experimentally observed behavior. We remark once again that the $\sigma(V_{\text{low-k}})$ shown in Fig. 4 should be essentially independent of the choice of a bare potential from which $V_{\text{low-k}}$ is derived (see subsection 4.1).

The above results correspond to the case where the four-momentum k of the exchanged pion is specified according to Eqs.(18) and (19). As discussed earlier, however, there is an argument that favors FKA in a certain context [32]. It therefore seems informative to repeat our calculation with the use of FKA. The σ corresponding to this case is shown in Fig. 5. We observe that the cross sections obtained in FKA are smaller than those in Fig. 4, representing a larger deviation from the experimental values, and that the energy dependence of σ does not resemble the experimentally observed behavior.

However, we need to discuss here the dependence of our results on the values of the LEC, c_1 , c_2 and c_3 . The above results were obtained for the “standard values” of c_1 , c_2 and c_3 given in Eq.(4). These were originally deduced in Ref. [28] and quoted in Ref. [7] as “parameter set I”. The allowed ranges of these LECs were discussed in Ref. [7, 29], where, in addition to the parameter set I, two more sets were considered as examples of other possible choices. For convenience, we tabulate these three sets of parameters:

Parameter set I

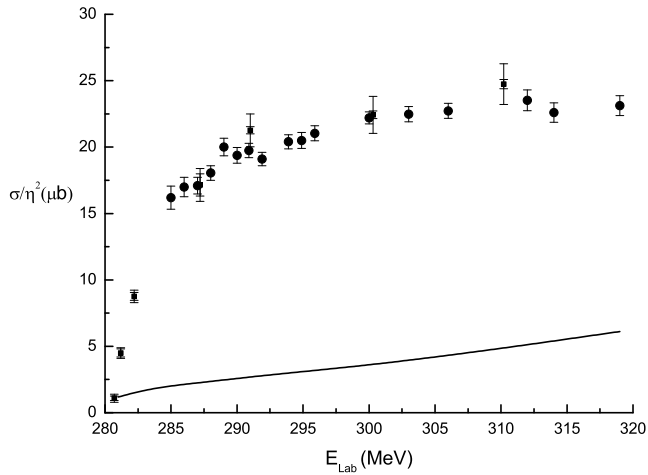


Figure 5: The total cross sections calculated from the full amplitude consisting of the impulse and rescattering terms evaluated in the *fixed kinematics approximation*. The experimental data points are taken from Ref. [14] (solid circles) and Ref. [15] (solid squares). For the explanation of the quantity η , see the caption of Fig.1.

$$c_1 = -0.87 \text{ GeV}^{-1}, \quad c_2 = 3.34 \text{ GeV}^{-1}, \quad c_3 = -5.25 \text{ GeV}^{-1} \quad (28)$$

Parameter set II

$$c_1 = -0.87 \text{ GeV}^{-1}, \quad c_2 = 4.5 \text{ GeV}^{-1}, \quad c_3 = -5.25 \text{ GeV}^{-1} \quad (29)$$

Parameter set III

$$c_1 = -0.98 \text{ GeV}^{-1}, \quad c_2 = 3.34 \text{ GeV}^{-1}, \quad c_3 = -5.25 \text{ GeV}^{-1}. \quad (30)$$

To get a measure of the sensitivity to the choice of the LECs, we have repeated our calculation of σ for $V_{\text{low-k}}$ using the parameter sets II and III. The results are shown in Fig. 6 together with those for the set I; in fact, since the set II gives practically the same result as the set I, we give in the figure only the results for the sets I and III. Fig. 6 indicates that the set III, which differs from the set I only by a modest 12% change in $c_1 = -0.98 \text{ GeV}^{-1}$, enhances σ considerably, bringing the calculated values of σ closer to the experimental values. However, the energy dependence of the theoretical σ remains dissimilar to the experimentally observed behavior. Figs. 4, 5 and 6 seem to suggest that, in order to fully explain the magnitude and incident-energy dependence of the $pp \rightarrow pp\pi^0$ cross sections near threshold, one probably needs to include terms of chiral orders higher than considered here. We remark in this connection that the possible importance of two-pion exchange diagrams in a χ PT calculation of the $pp \rightarrow pp\pi^0$ reaction was pointed out in Refs. [35, 36].

5 Discussion and Summary

We have carried out a hybrid χ PT calculation of the cross section σ for the s -wave pion production reaction, $pp \rightarrow pp\pi^0$, with the use of $V_{\text{low-k}}$. $V_{\text{low-k}}$ is a low-energy effective potential derived from a high-precision phenomenological potential (called a “bare” potential in our context) by integrating out momentum components higher than $\Lambda \sim 2 \text{ fm}^{-1}$. The results obtained with $V_{\text{low-k}}$ are compared with those obtained with the three representatives bare potentials, ANL V18, Bonn-B and CD-Bonn.

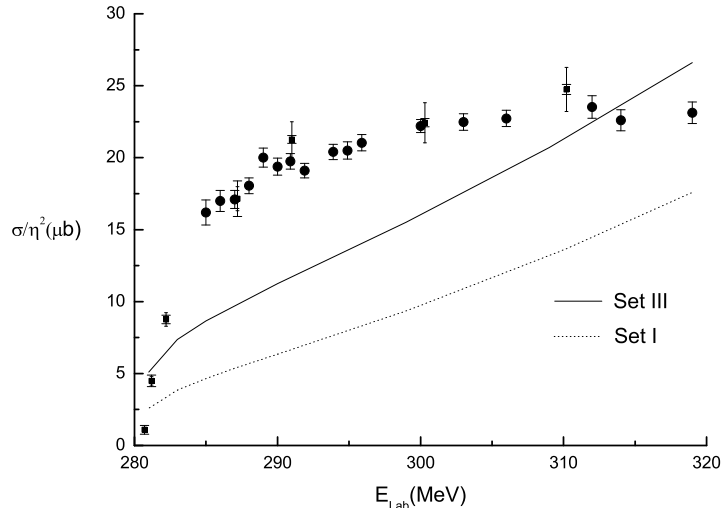


Figure 6: The total cross section σ calculated with the full amplitude (including both the one-body and two-body amplitudes) for $V_{\text{low-k}}$. The results obtained with the parameter sets I and III are compared. The experimental data points are taken from Ref. [14] (solid circle) and Ref. [15] (solid square).

The principal features of our calculation based on $V_{\text{low-k}}$ are summarized as follows.

- (1) A hybrid χ PT calculation based on a bare potential has the “momentum mismatch” problem that the initial and final nuclear wave functions generated by the bare potential involve very high momenta, whereas the transition operators derived from χ PT can be used only within a limited momentum range ($p \leq 300$ MeV). This momentum mismatch problem is significantly mitigated by the use of $V_{\text{low-k}}$.
- (2) Reflecting the fact that the short-distance behavior of the bare potential is not well controlled, the σ 's calculated with the above-mentioned three bare potentials exhibit $\sim 40\%$ variance. This kind of model dependence practically disappears with the use of $V_{\text{low-k}}$, since different choices of a bare potential lead to practically equivalent $V_{\text{low-k}}$'s [26]. This feature allows us to better focus on the question whether the transition operator for the $pp \rightarrow pp\pi^0$ reaction derived from χ PT up to next-to-leading order is adequate or not.
- (3) The calculation with $V_{\text{low-k}}$ enhances σ over the values obtained with the bare potentials, and, with certain choices of the relevant LECs, σ can come close to the experimental values for some range of the incident energy. It is however unlikely that the magnitude and energy dependence of σ can be fully reproduced with the transition operators considered in this work. Thus it seems necessary to consider higher-order transition operators.

For formal consistency, it is desirable to go beyond the hybrid χ PT approach by employing N-N potentials derived from χ PT. This is however a major task relegated to the future. We remark in this connection that, for reactions that only involve the rearrangement of the nucleons, there has been much progress in constructing a framework that is formally consistent with effective field theory [37, 38].

A related issue is that we concentrated here on the consequences of changing the nuclear wave functions from those generated by the bare NN potentials to those generated by $V_{\text{low-k}}$, *without* taking account of the possible renormalization of the transition operators due to the truncation of model space.⁶ As is well known, a reduction of nuclear model space in general entails a corresponding modification of

⁶For discussion of some formal aspects of the use of $V_{\text{low-k}}$ in hybrid χ PT, see Ref. [39].

operators for the nuclear observables. Again, to fully address this issue, we need to go beyond the hybrid χ PT used in this work. In the present study of exploratory nature, we have concentrated on a hybrid χ PT evaluation of the transition operators that arise from the tree diagrams. At this chiral order there are no loop corrections to the LECs (c_i , $i = 1, 2, 3$) and the other coefficients appearing in \mathcal{L}_{ch} like, e.g. g_A . We may therefore expect that, although the scale of χ PT ($\Lambda_\chi \sim 1$ GeV) is larger than the momentum cutoff scale ($\Lambda \sim 2$ fm $^{-1}$) used in deriving $V_{\text{low-k}}$, this difference does not lead to a drastic renormalization of the transition operators. To turn around the argument, the issue of the renormalization of the transition operators is coupled with the treatment of higher chiral-order terms, and these two aspects need to be addressed simultaneously. This important question, however, is beyond the scope of our present study, which is limited to the tree diagrams.

As an immediate follow-up of the work described here, we are studying [40] the expected important contributions from the two-pion exchange diagrams [35, 36] in a hybrid χ PT calculation with $V_{\text{low-k}}$.

6 Acknowledgment

We are grateful to T.T.S. Kuo for generously allowing us to use the $V_{\text{low-k}}$ code. We are also grateful to R. Machleidt for providing the USC group with a code to test the Bonn-B potential, and also for sending the CD-Bonn code used in this work to the Osaka University group. We are appreciative of the insightful comments we received from S. Ando and C. Hanhart. This work is supported in part by the US National Science Foundation, Grant Nos. PHY-0140214 and PHY-0457014. TS gratefully acknowledges financial support from the Japan Society for the Promotion of Science, Grant-in-Aid for Scientific Research (C) 15540275.

Appendix A

With the use of $V_{\text{low-k}}$, the numerical evaluation of the second integral of the impulse amplitude [Eq.(27)] requires the “modified” Bessel transformation,

$$R_{(LS)J,p_0}(r) = \sqrt{\frac{2}{\pi}} i^L \int_0^\Lambda p^2 dp j_L(pr) R_{(LS)J,p_0}(p). \quad (31)$$

However, since $\int_0^\Lambda j_L(pr) j_L(pr') p^2 dp \neq \frac{\pi}{2r^2} \delta(r - r')$, the inverse transformation for Eq.(31) gets complicated, which presents us from arriving at an r-space expression similar to Eq.(26). We therefore replace $R_{(LS)J,p_0}(p)$ in Eq.(31) with the K-matrix expression Eq.(17) and then we use in Eq.(27) the Bessel transformation

$$R_{(LS)J,p_0}(k) = \sqrt{\frac{2}{\pi}} i^{-L} \int_0^\infty r^2 dr j_L(kr) R_{(LS)J,p_0}(r), \quad (32)$$

where $k \leq \Lambda$ is understood. In our numerical evaluation of the impulse amplitude with $V_{\text{low-k}}$, only the initial wave function in the second integral of Eq.(27) is evaluated using the above prescription.

Appendix B

To check the validity of the numerical techniques described in the text, it is informative to compare the σ^{Imp} calculated for $V_{\text{low-k}}$ using the prescription explained in subsection 3.2 with the σ^{Imp} obtained

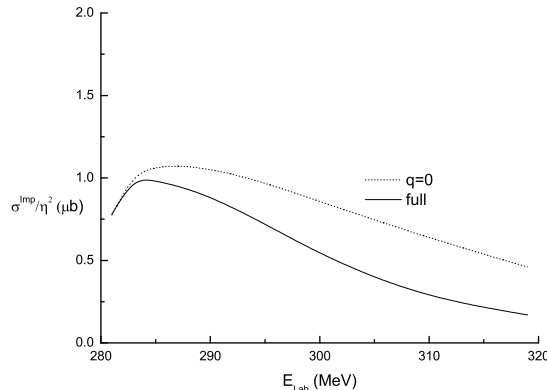


Figure 7: σ^{Imp} calculated for $V_{\text{low-k}}$ without or with the $\vec{q} = 0$ approximation. The solid (dotted) line corresponds to the calculation without (with) $\vec{q} = 0$ approximation. For the explanation of the quantity η , see the caption of Fig.1.

in the “ $\vec{q} = 0$ approximation”, wherein the transition operators are derived under the simplifying assumption that the out-going pion has no momentum, $\vec{q} = 0$. [In evaluating the phase space, we do treat \vec{q} as a variable.] In the $\vec{q} = 0$ approximation, the impulse term can be evaluated in p-space in a straightforward manner without any complicated handling of the principal value integrals. The results for the two cases, with and without the $\vec{q} = 0$ approximation, are shown in Fig. 7, and we compare this figure with Fig. 2 in Ref. [7], which presents σ^{Imp} calculated for the bare potentials with and without the $\vec{q} = 0$ approximation. According to Fig. 2 in Ref. [7], σ^{Imp} obtained in the $\vec{q} = 0$ approximation tends to become somewhat larger than σ^{Imp} obtained without using the $\vec{q} = 0$ approximation. The fact that Fig. 7 exhibits a similar tendency may be taken as an indication that the somewhat lengthy procedure we use in handling the principal-value integrals for the $V_{\text{low-k}}$ case is reliable.

References

- [1] T.-S. H. Lee and D. O. Riska, Phys. Rev. Lett. **70**, 2237 (1993); see also C. J. Horowitz, H. O. Meyer and D. K. Griegel, Phys. Rev. C **49**, 1337 (1994).
- [2] E. Hernández and E. Oset, Phys. Lett. **B350**, 158 (1995).
- [3] C. Hanhart, J. Haidenbauer, A. Reuber, C. Schütz and J. Speth, Phys. Lett. **B358**, 21 (1995).
- [4] B.-Y. Park, F. Myhrer, T. Meissner, J.R. Morones, K. Kubodera, Phys. Rev. **C53**, 1519 (1996).
- [5] T.D. Cohen, J.L. Friar, G.A. Miller and U. van Kolck, Phys. Rev. **C53**, 2661 (1996).
- [6] U. van Kolck, G. A. Miller and D. O. Riska, Phys. Lett. **B388**, 679 (1996).
- [7] T. Sato, T.-S. H. Lee, F. Myhrer and K. Kubodera, Phys. Rev. **C56**, 1246 (1997).
- [8] S. Ando, T.-S. Park and D.-P. Min, Phys. Lett. B, **509**, 253 (2001)
- [9] C. Hanhart, J. Haidenbauer, O. Krehl, J. Speth, Phys. Lett. **B444**, 25 (1998)

- [10] E. Gedalin, A. Moalem, L. Razdolskaya, Phys. Rev. **C60**, 031001 (1999)
- [11] C. Hanhart, U. van Kolck, G.A. Miller, Phys. Rev. Lett. **85**, 2905 (2000).
- [12] V. Malafaia and M.T. Peña, Phys. Rev. **C69**, 024001 (2004); V. Malafaia, J. Adam Jr. and M.T. Peña, Phys. Rev. **C71**, 034002 (2005).
- [13] C. Hanhart, Phys. Rept. **397**, 155 (2004).
- [14] H. O. Meyer *et al.*, Phys. Rev. Lett. **65**, 2846 (1990); Nucl. Phys. **A539**, 633 (1992).
- [15] A. Bondar *et al.*, Phys. Lett. **B356**, 8 (1995).
- [16] D.S. Koltun and A. Reitan, Phys. Rev. **141**, 1413 (1966).
- [17] G. A. Miller and P. U. Sauer, Phys. Rev. C **44**, R1725 (1991); J.A. Niskanen, Phys. Lett. **B289**, 227 (1992)
- [18] T.-S. Park, D.-P. Min and M. Rho, Phys. Repts. **233**, 341 (1993); T.-S. Park, I.S. Towner and K. Kubodera, Nucl. Phys. **A 579**, 381 (1994); T.-S. Park, D.-P. Min and M. Rho, Phys. Rev. Lett. **74**, 4153 (1995); Nucl. Phys. **A596**, 515 (1996).
- [19] T.-S. Park, K. Kubodera, D.-P. Min and M. Rho, Phys. Rev. C, **58**, 637 (1998); Astrophys. J. **507**, 443 (1998); Nucl. Phys. A, **646**, 83 (1999); Phys. Lett. B, **472**, 232 (2000); Nucl.Phys. A (Proc. Suppl.), **684**, 101 (2001).
- [20] T.-S. Park et al., Phys. Rev. C, **67**, 055206 (2003); see also T.-S. Park et al, nucl-th/0106025;nucl-th/0107012.
- [21] S. Ando et al., Phys. Lett. B, **555**, 49 (2003).
- [22] K. Kubodera and T.-S. Park, Annu. Rev. Nucl. Part. Sci. **54**, 19 (2004).
- [23] R.B. Wiringa, V.G.J. Stoks and R. Schiavilla, Phys. Rev. **C51**, 38 (1995).
- [24] R.V. Reid Jr., Ann. Phys. **50**, 411 (1968)
- [25] S. Bogner, T.T.S. Kuo and L. Coraggio, Nucl. Phys. **A684**, 432c (2001); S. Bogner, T.T.S. Kuo, L. Coraggio, A. Covello and N. Itaco, Phys. Rev. C, **65**, 051301 (2002).
- [26] S. Bogner, T.T.S. Kuo and A. Schwenk, Phys. Rept. **386**, 1 (2003)
- [27] E. Jenkins and A. V. Manohar, Phys. Lett. **B255**, 558 (1991).
- [28] For a review, see e.g., V. Bernard, N. Kaiser and U.-G. Meissner, Int. J. Mod. Phys. **E4**, 193 (1995)
- [29] V. Bernard, N. Kaiser and U.-G. Meissner, Nucl. Phys. A, **615**, 483 (1997).
- [30] S. Weinberg, Phys. Lett. **B251**, 288 (1990); Nucl. Phys. **B363**, 3 (1991); Phys. Lett. **B295**, 114 (1992).
- [31] M. Haftel and F. Tabakin, Nucl. Phys. **A158**, 1 (1970).

- [32] C. Hanhart, G.A. Miller, F. Myhrer, T. Sato and U. van Kolck, Phys. Rev. **C 63**, 044002 (2001).
- [33] R. Machleidt, Phys. Rev. C, **63**, 024001 (2001).
- [34] R. Machleidt, *Computational Nuclear Physics 2 – Nuclear Reactions*, K. Langanke, J.A. Maruhn, and S.E. Koonin, eds. (Springer, New York, 1993), pp. 1-29.
- [35] V. Dmitrašinović, K. Kubodera, F. Myhrer and T. Sato, Phys. Lett. **B465**, 43 (1999)
- [36] C. Hanhart and N. Kaiser, Phys. Rev. **C66**, 054005 (2002)
- [37] E. Epelbaum et al., Nucl. Phys. A, **645**,413 (1999); E. Epelbaum, W. Gloeckle and U.-G. Meissner, Nucl. Phys. A, **671**, 295 (2000); E. Epelbaum et al., Phys. Rev. Lett. **86**, 4787 (2001); E. Epelbaum et al., Phys. Rev. C, **66**, 064001 (2002); Eur. Phys. J. A, **15**, 543 (2002).
- [38] P.F. Bedaque and U. van Kolck, Annu. Rev. Nucl. Part. Sci. **52**, 339 (2002).
- [39] S. Nakamura, preprint nucl-th/0411109.
- [40] Y. Kim, K. Kubodera, F. Myhrer and T. Sato, work in progress.